



Modelled interglacial carbon cycle dynamics during the Holocene, the Eemian and Marine Isotope Stage (MIS) 11

Thomas Kleinen¹, Victor Brovkin¹, and Guy Munhoven²

¹Max Planck Institute for Meteorology, Bundesstr. 53, 20146 Hamburg, Germany

²LPAP, Institut d'Astrophysique et de Géophysique, Université de Liège, Liège, Belgium

Correspondence to: Thomas Kleinen (thomas.kleinen@mpimet.mpg.de)

Received: 22 April 2015 – Published in Clim. Past Discuss.: 20 May 2015

Revised: 14 October 2016 – Accepted: 18 October 2016 – Published: 29 November 2016

Abstract. Trends in the atmospheric concentration of CO₂ during three recent interglacials – the Holocene, the Eemian and Marine Isotope Stage (MIS) 11 – are investigated using an earth system model of intermediate complexity, which we extended with process-based modules to consider two slow carbon cycle processes – peat accumulation and shallow-water CaCO₃ sedimentation (coral reef formation). For all three interglacials, model simulations considering peat accumulation and shallow-water CaCO₃ sedimentation substantially improve the agreement between model results and ice core CO₂ reconstructions in comparison to a carbon cycle set-up neglecting these processes. This enables us to model the trends in atmospheric CO₂, with modelled trends similar to the ice core data, forcing the model only with orbital and sea level changes. During the Holocene, anthropogenic CO₂ emissions are required to match the observed rise in atmospheric CO₂ after 3 ka BP but are not relevant before this time. Our model experiments show a considerable improvement in the modelled CO₂ trends by the inclusion of the slow carbon cycle processes, allowing us to explain the CO₂ evolution during the Holocene and two recent interglacials consistently using an identical model set-up.

have been active during all interglacials. While the Holocene CO₂ trend has generated considerable interest previously (Ruddiman, 2003), the context of previous interglacials has been neglected in process-based carbon cycle model studies. The present study aims at filling this gap.

Investigations of the Holocene trend in CO₂ can be classified into two basic approaches: an inverse modelling approach and a forward or process-based modelling approach. The inverse modelling approach takes the ice core record of CO₂ and $\delta^{13}\text{CO}_2$ as a starting point and aims at deriving the sources and sinks of CO₂ from this record, while the forward modelling approach starts from the carbon cycle processes and aims at determining a CO₂ trajectory from combinations of these.

Following the inverse modelling approach, based on records of CO₂ and its stable carbon isotopic ratio $\delta^{13}\text{CO}_2$ from ice cores, Indermühle et al. (1999) deconvolved the mass balance equations for CO₂ and $\delta^{13}\text{CO}_2$ to solve for the unknown terrestrial and oceanic sources and sinks of CO₂. They explained the changes in atmospheric CO₂ by major contributions from decreases in land carbon (C) storage and changes in sea surface temperature (SST), while changes in the cycling of CaCO₃ played only a minor role. This approach was subsequently refined by Elsig et al. (2009), who presented atmospheric $\delta^{13}\text{CO}_2$ records with higher resolution and better precision. They attributed the change in atmospheric CO₂ between 8 ka BP and the pre-industrial period to carbonate compensation induced by earlier land-biosphere uptake as well as coral reef formation, with some contribution from carbon released from the land biosphere.

Using the forward modelling approach, Ridgwell et al. (2003) used estimates of deep ocean carbonate ion con-

1 Introduction

The atmospheric concentration of carbon dioxide (CO₂) increased from 260 to 280 ppm CO₂ during the Holocene between 8 ka BP and the pre-industrial period. This trend in CO₂ has to be seen in the context of previous interglacials, since all processes affecting the atmospheric concentration, with the exception of possible human influences, are likely to

centrations to constrain the carbon cycle. They found that the observed trend in atmospheric CO₂ during the last 8000 years can best be explained by the build-up of coral reefs and other forms of shallow-water carbonate deposition. Joos et al. (2004), employing the Bern carbon cycle climate model to simulate the interval from the Last Glacial Maximum (LGM) to the pre-industrial period, found that a combination of processes contributed to the Holocene rise in CO₂, with carbonate compensation in response to terrestrial vegetation regrowth, SST changes and coral reef build-up playing a role. On the other hand, Brovkin et al. (2002), as well as Menviel and Joos (2012), found almost no effect of SST changes on CO₂ during the Holocene.

Kleinen et al. (2010), using the CLIMBER2-LPJ model, showed that the trend in atmospheric CO₂ over the Holocene is controlled by the balance of two slow processes: (1) carbon uptake by boreal peatlands, which is (slightly over-) compensated for by (2) the outgassing of CO₂ due to the accumulation of CaCO₃ in shallow oceanic areas. Finally, Menviel and Joos (2012) investigated the Holocene CO₂ rise by applying the Bern3D ocean carbon cycle model, with prescribed scenarios of shallow-water carbonate accumulation and land C uptake. In their experiments, shallow-water carbonate accumulation, land carbon uptake and release, and the consecutive carbonate compensation response, as well as the response of the ocean-sediment system to marine changes during the termination, contribute roughly equally to the CO₂ rise.

For earlier interglacials, investigations are rare. Schurgers et al. (2006) investigated the changes in atmospheric CO₂ during the Holocene and during the Eemian using the ECHAM3-LSG general circulation model (GCM), including the dynamic global vegetation model (DGVM) LPJ and the marine biogeochemistry model HAMOCC3. They found increases in atmospheric CO₂ for both the Eemian and the Holocene, mainly driven by decreases in terrestrial C storage. They were, however, unable to explain the overall magnitude of the CO₂ trend during the Holocene, and their positive trend in atmospheric CO₂ during the Eemian is different from that in the ice core data, which actually show no trend.

In the present publication we improve on the study by Kleinen et al. (2010) in two respects: (1) both the accumulation of peatland carbon and the burial of CaCO₃ were scenarios and not modelled interactively, and (2) the study only considered the Holocene, while neglecting to show that the same mechanisms can also explain the evolution of CO₂ during previous interglacials. Our model now includes a dynamic peatland model, as well as a dynamic model of carbonate accumulation by coral reefs, which finally enables us to consistently investigate the evolution of atmospheric CO₂ during the Holocene and during two interglacials that preceded it: the Eemian and Marine Isotope Stage (MIS) 11. The Holocene and the Eemian are particularly interesting because validation data of reasonable time resolution and reliability are available for these interglacials. We did not investigate in-

terglacials prior to MIS 5 since no $\delta^{13}\text{C}$ CO₂ data are available for validation, with the exception of MIS 11 since its unusual length makes it a particularly interesting case and ice core CO₂ data of reasonable time resolution are still available. We investigate to what extent the evolution of CO₂ during these three different interglacials can be explained by the interplay of two slow carbon cycle processes: peat accumulation and CaCO₃ accumulation in shallow waters.

2 Model and experiments

2.1 The model

To investigate these questions we are using CLIMBER2-LPJ, which consists of the earth system model of intermediate complexity (EMIC) CLIMBER2, coupled to the DGVM LPJ. This combination of models allows experiments on timescales of an interglacial due to the low computational cost of CLIMBER2, while accounting for the heterogeneity of land surface processes on the much finer grid of LPJ.

CLIMBER2 (Petoukhov et al., 2000; Ganopolski et al., 2001) consists of a 2.5-dimensional statistical–dynamical atmosphere with a latitudinal resolution of 10° and a longitudinal resolution of roughly 51°, an ocean model resolving three zonally averaged ocean basins with a latitudinal resolution of 2.5°, a sea ice model, and the dynamic terrestrial vegetation model VECODE (Brovkin et al., 2002). In the present model experiments, the latter model is used only for determining biogeophysical responses to climate change (i.e. as a land surface scheme for the climate model), while biogeochemical effects, i. e., the corresponding carbon fluxes, are determined by LPJ. VECODE and LPJ produce similar vegetation changes, and discrepancies therefore are very small.

CLIMBER2 also contains an oceanic biogeochemistry model (Ganopolski et al., 1998; Brovkin et al., 2002, 2007) and a sediment model that describes the diffusive pore-water dynamics, assuming oxic-only respiration and 4.5-order CaCO₃ dissolution kinetics (Archer, 1991; Brovkin et al., 2007). Volcanic emissions of CO₂ are assumed to be constant at 0.07 Gt C a⁻¹ (Gerlach, 2011). Weathering fluxes scale to runoff from the land surface grid cells, with separate carbonate and silicate lithological classes. The long-term carbon cycle that includes the processes of deep-sea and shallow-water carbonate accumulation, weathering and volcanic outgassing is brought to equilibrium for the pre-industrial climate as in Brovkin et al. (2012).

We have coupled the DGVM LPJ (Sitch et al., 2003; Gerten et al., 2004) to CLIMBER-2 in order to investigate land surface processes at a resolution significantly higher than that of CLIMBER2. We also extended the model by implementing carbon isotope fractionation according to Scholze et al. (2003). LPJ is run on a 0.5° × 0.5° grid and is called at the end of every model year simulated by CLIMBER2. Anomalies from the climatology of the temperature, precipitation and cloudiness fields are passed to LPJ,

where they are added to background climate patterns based on the CRU-TS climate data set (New et al., 2000). In order to retain some temporal variability in these climate fields, the anomalies are not added to the climatology of the CRU-TS data set, but rather to the climate data for 1 year randomly drawn from the range 1901–1930. The change in the LPJ carbon pools is then passed back to CLIMBER2 as the carbon flux F_{AL} between atmosphere and land surface and is employed to determine the atmospheric CO_2 concentration for the next model year.

2.2 Accumulation of calcium carbonate in shallow waters

The accumulation of CaCO_3 in shallow waters leads to an increase in the atmospheric CO_2 concentration. The production of CaCO_3 proceeds following the carbonate precipitation equation $\text{Ca}^{2+} + 2\text{HCO}_3^- \rightarrow \text{CaCO}_3 + \text{CO}_2 + \text{H}_2\text{O}$. Under present conditions in seawater about 0.6 mol of CO_2 will be released for every mol of CaCO_3 produced (Frankignoulle et al., 1994). This is implicitly handled by the carbonate speciation and air–sea gas exchange routines.

The marine carbon cycle in CLIMBER2 has been extended by a model of carbonate accumulation in shallow waters, which was derived from the ReefHab model (Kleypas, 1997). The original ReefHab predicts reef habitat area and accumulation of CaCO_3 in these environments as a function of temperature, salinity, nutrients and light. The model considers corals as the main shallow-water carbonate producers, but it is also applicable to calcareous algae, which have calcification rates very similar to corals.

For the implementation in CLIMBER2, we determined the potential reef area A by diagnosing the sea floor area above the maximum depth of reef growth for each ocean grid cell, depending on the global sea level, from the ETOPO2 data set (US Dept. of Commerce, 2006). In addition, we determined the topographic relief function TF , as described by Kleypas (1997). We then determine the vertical coral accumulation rate according to Kleypas (1997) as $G = G_{\max} \tanh(I_z / I_k)$, with G_{\max} the maximum accumulation rate, I_z the photosynthetically active radiation (PAR) at depth z and I_k the saturating light intensity necessary for photosynthesis. We calculate G for all grid cells where $\text{SST} > 18.1$ and < 31.5 °C, the growth limits for corals (Kleypas, 1997).

In the original Kleypas (1997) model, sea level is only used to calculate the area available for shallow-water sedimentation, but the rate of sea level change is not considered in calculating the rate of CaCO_3 sedimentation. However, the rate of CaCO_3 accumulation by coral reefs will be strongly perturbed during periods of sea level drop or very fast sea level rise. A moderate rate of sea level rise, on the other hand, can maximize coral reef build-up. We therefore implemented a dependence of the CaCO_3 sedimentation rate on the rate of sea level change based on Munhoven and François (1996). Munhoven and François (1996) con-

sider a trapezoidal growth-limiting function Θ , which restricts the coral reef growth in the case of sea level rising too fast or falling. According to Buddemeier and Smith (1988) the best overall estimate for the sustained maximum rate of reef growth is 10 mm a^{-1} . For simplicity, we therefore adopt 0 and 10 mm a^{-1} as the limiting sea level rates. To avoid changes that are too abrupt, accumulation rates are reduced from 100 to 0 % of the normal rate (from 10 to 15 mm a^{-1}); similarly we let them increase from 0 to 100 %, i.e. from -2.5 (i.e. a 2.5 mm a^{-1} decrease) to $+2.5 \text{ mm a}^{-1}$. We thus allow for a small accumulation as long as sea level falls only slowly. Carbonate accumulation rates will not drop to zero immediately since corals may live even at depths of 50 m and more, and their habitat therefore does not vanish immediately.

The total CaCO_3 accumulation in each grid cell where ocean temperature is within the acceptable range therefore is $P = G \times \Theta \times A \times TF$, which we sum up for all grid cells to determine the total shallow-water CaCO_3 accumulation. Total accumulation is scaled to conform to the Milliman (1993) estimate of shallow-water CaCO_3 accumulation for the late Holocene. Milliman (1993) estimates a shallow-water carbonate accumulation rate of about 1.5 billion tonnes of CaCO_3 per year, which converts to 15 Tmol a^{-1} . The area factors A and TF are more or less constant over the sea level range of our experiments. Therefore, variations in CaCO_3 formation are primarily due to variations in the rate of sea level change. In experiments where the dynamic calculation of CaCO_3 sedimentation is disabled, a constant shallow-water CaCO_3 sedimentation flux of 2 Tmol a^{-1} is prescribed to balance the oceanic alkalinity budget.

2.3 Carbon accumulation in peatlands

According to Yu et al. (2010), global peatlands store about 615 Pg of carbon in the form of peat soils: northern high-latitude peatlands account for about 550 Pg C, tropical peatlands for about 50 Pg C and southern peatlands for about 15 Pg C. This carbon has largely been accumulated since the LGM.

In order to account for this accumulation of carbon, we have extended CLIMBER2-LPJ by the dynamic model of peatland extent and peat carbon accumulation of Kleinen et al. (2012). The model determines peatland extent from topography and climatic conditions. In the peatland areas obtained it accumulates carbon due to the slow decomposition of C under the anaerobic conditions in peatlands. For the last 8 kyr, this model calculates an accumulation of 330 Pg C in high northern latitude areas, which is roughly in line with the Yu et al. (2010) estimate of 550 Pg C for the time period from the LGM to the present (Kleinen et al., 2012). The main factor influencing the uncertainty of this model result is the peatland area estimate. Kleinen et al. (2012) considered minimum and maximum area estimates from which they derived an uncertainty range of 240–490 Pg C for the peat ac-

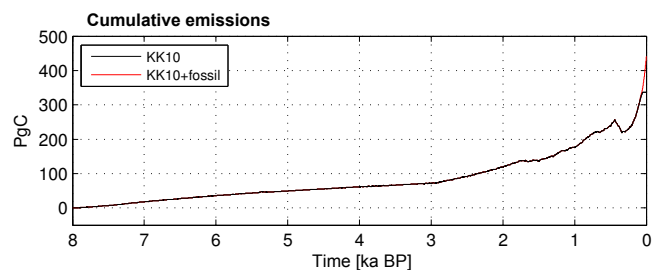


Figure 1. Cumulative carbon emissions from land use (Kaplan et al., 2011; black) and land use and fossil fuel (Meinshausen et al., 2011; red).

cumulation between 8 and 0 ka BP, with a most likely value of 330 Pg C.

Tropical peatlands could, unfortunately, not be considered in the present experiments, due to the lack of reliable calibration data for tropical peatlands. Preliminary model experiments indicate that the carbon stock in tropical peatlands has not varied over the Holocene though. We therefore assume that we introduce no major errors by neglecting them. Furthermore, they represent less than 10 % of the total, according to the figures from Yu et al. (2010). It should be noted that experiments in which peat accumulation is considered display a decreased total carbon stock for soil carbon in mineral soils in comparison to the experiments where peat accumulation is not considered. In the former type of experiments the area covered by mineral soils is smaller since part of a grid cell may be set aside for peatlands. The offset in total carbon stocks between the experiments with and without consideration of peat carbon accumulation therefore does not reflect a different carbon density in any particular location, but rather the reduced area of mineral soils.

2.4 Forcing data

The model is forced by orbital changes following Berger (1978) in all experiments. For the experiments that include shallow-water CaCO_3 accumulation, we also force the model by providing sea level data. We obtained the sea level, as well as the rate of sea level change, from a previous experiment performed with CLIMBER2 coupled to the ice sheet model SICOPOLIS, run over the last eight glacial–interglacial cycles (Ganopolski and Calov, 2011). The sea level change in these experiments is mainly derived from changes in the Northern Hemisphere (NH) ice sheets, though changes in Antarctic ice sheet size are considered by assuming that these are 10 % of the NH changes. The global ice sheet volume obtained compares well with the reconstruction of sea level by Waelbroeck et al. (2002).

One model experiment for the Holocene is also forced with anthropogenic carbon emission data. We obtained a scenario of carbon emissions from land use changes from Kaplan et al. (2011), who reconstructed global changes in land

use over the last 8000 years and provided a scenario of corresponding carbon emissions. The scenario is called KK10. It covers the time from 8 ka BP to AD 1900, and we extend it to 1950 with land use from the representative concentration pathway (RCP) scenario database (Meinshausen et al., 2011).

After AD 1765 (or 185 BP) we also add historical emissions from fossil fuel use from the RCP database (Meinshausen et al., 2011). The adopted cumulative emissions are shown in Fig. 1. For simplicity, CO_2 emissions from land use changes are directly added to the atmospheric CO_2 ; i.e. we do not change the land carbon stocks when CO_2 is emitted from land use changes. This simplification will lead to a slight overestimate of the carbon uptake by vegetation through CO_2 fertilization. We nevertheless judge the impact of this simplification to be minor. Both land use and fossil fuel emissions are assumed to have a $\delta^{13}\text{C}_{\text{CO}_2}$ of -25‰ .

2.5 Ice core data

We compare the atmospheric CO_2 concentrations from our experiments to CO_2 concentration reconstructions from ice cores. We use the recent compilation by Bereiter et al. (2015), which consists of data from Law Dome (Rubino et al., 2013; MacFarling Meure et al., 2006) and the European Project for Ice Coring in Antarctica (EPICA) Dome C (EDC; Monnin et al., 2001, 2004) for the Holocene, data from EDC (Schneider et al., 2013) for the Eemian, and data from Vostok (Petit et al., 1999) and EDC (Siegenthaler et al., 2005) for MIS 11. The data are on the AICC2012 timescale (Bazin et al., 2013), with the exception of the data from Law Dome.

For $\delta^{13}\text{C}_{\text{CO}_2}$, we compare the Holocene results to the compilation by Schmitt et al. (2012), based on data obtained from EDC by Elsig et al. (2009) and Laurantou et al. (2010), and we compare the Eemian results to data from Schneider et al. (2013). For both time frames, we compare results to both the original data and to the Monte Carlo average, which should remove most of the analytical uncertainties.

2.6 Model experiments

Due to its long memory the carbon cycle is not in equilibrium at any particular point in time during an interglacial. The best approach to investigate the carbon cycle during an interglacial would therefore be to perform a model simulation of several glacial cycles. This would ensure that the carbon cycle is equilibrated to the time-varying boundary conditions as much as possible. Unfortunately, this approach is not yet feasible, in particular because of computational constraints. We therefore aim to initialize the model to conditions early in the interglacial but after the large transient changes associated with the deglaciation are over. For the Holocene this implies starting the model simulation at 8 ka BP, when most of the ice sheets have melted and the initial regrowth of vegetation is finished. For the Eemian we begin the model ex-

Table 1. Set-up of experiments performed for the interglacials, including the forcing factors varied.

Name	Interglacial	Initial CO ₂ (ppm)	Initial $\delta^{13}\text{CO}_2$ (‰)	Initial time (ka BP)	Peat	Coral CaCO ₃	Anthropogenic emissions
HOL_ORB	Holocene	260	-6.4	8	No	No	No
HOL_PEAT	Holocene	260	-6.4	8	Yes	No	No
HOL_NAT	Holocene	260	-6.4	8	Yes	Yes	No
HOL_MPT	Holocene	260	-6.4	8	Minimum	Yes	No
HOL_ANT	Holocene	260	-6.4	8	Yes	Yes	Yes
EEM_ORB	Eemian	276	-6.7	126	No	No	No
EEM_NAT	Eemian	276	-6.7	126	Yes	Yes	No
MIS11_ORB	MIS11	271	-6.5	420	No	No	No
MIS11_NAT	MIS11	271	-6.5	420	Yes	Yes	No

periment at 126 ka BP, after the large transient peak in CO₂ has decayed, and for MIS 11 we start the model at 420 ka BP. From these starting points onward, we drive the model with orbital and other forcings as appropriate until the end of the experiment at 0 ka, 116, and 380 ka BP for the Holocene, the Eemian and MIS 11, respectively.

Since the carbon cycle cannot be regarded as being in equilibrium on multi-millennial timescales, we initialized the model for our experiments with a similar procedure as in Kleinen et al. (2010). Firstly, the model was run with equilibrium conditions appropriate for the beginning of the respective interglacial, including constant CO₂ as diagnosed from ice cores for that time. Atmospheric $\delta^{13}\text{CO}_2$ was also initialized to the ice core value. In a second step, ocean alkalinity was increased to get a carbonate sedimentation flux of 16 Tmol a⁻¹ in the deep ocean and 2 Tmol a⁻¹ on the shelves in order to simulate the maximum in CaCO₃ preservation in the deep sea before the onset of the interglacial. The model was then run with prescribed CO₂ for 5000 years. This set-up of initial conditions ensures that the ocean biogeochemistry is in equilibrium with the climate at the onset of the interglacial, while it is in transition from the glacial to interglacial state thereafter. Initial times and CO₂ concentrations are summarized in Table 1. After the climate model state for the beginning of the model experiment has been obtained, this climate state is used for a separate offline spin-up of the LPJ DGVM to determine an appropriate vegetation distribution and land carbon storage for the beginning of the experiment. The length of this spin-up is 2000 years.

Using these initial conditions, we then perform our experiments for the Holocene, the Eemian and MIS 11. For the Holocene, we perform five experiments to investigate the role of the various forcings in the interglacial carbon cycle: (1) HOL_ORB, an experiment in which neither peat accumulation nor CaCO₃ sedimentation nor anthropogenic land use emissions but only orbital forcing is considered; (2) HOL_PEAT, an experiment in which peat accumulation but neither CaCO₃ sedimentation nor anthropogenic land use emissions are considered; (3) HOL_NAT, an ex-

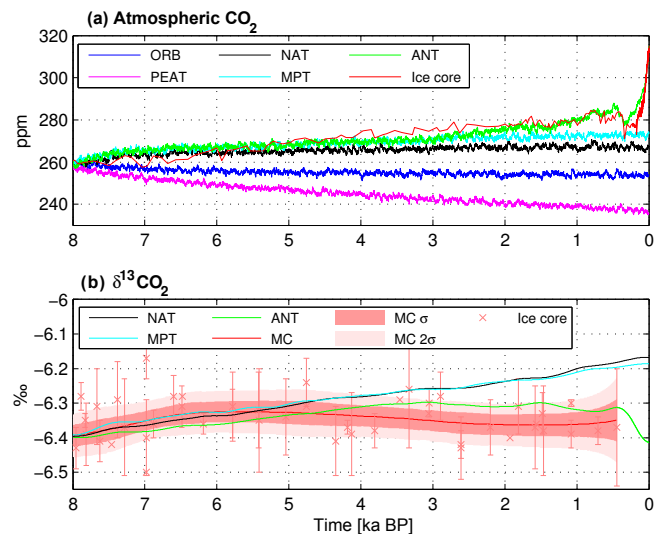


Figure 2. Holocene CO₂ concentration (a) and $\delta^{13}\text{CO}_2$ (b) from model experiments and ice core data. $\delta^{13}\text{CO}_2$ model results have been smoothed for clarity and offset, as described in the text. Ice core CO₂ data are from Law Dome and EDC as compiled by Bereiter et al. (2015). $\delta^{13}\text{CO}_2$ data are from EDC (Elsig et al., 2009), with Monte Carlo average (MC) and uncertainty estimate (MC σ ; Schmitt et al., 2012).

periment where all of the natural forcing mechanisms, i.e. peat accumulation and CaCO₃ sedimentation, are considered; (4) HOL_MPT, an experiment where all the natural forcing mechanisms are considered (as in HOL_NAT) but in which the minimum peatland area estimate from Kleinen et al. (2012) is used; (5) HOL_ANT, which again uses the same forcings as HOL_NAT, but also includes anthropogenic carbon emissions. For each of the Eemian and MIS11, we performed two experiments analogous to HOL_ORB and HOL_NAT, with adapted initial conditions. The characteristics of all experiments are summarized in Table 1.

All experiments are driven by orbital changes (Berger, 1978). In the experiments that consider variable shallow-

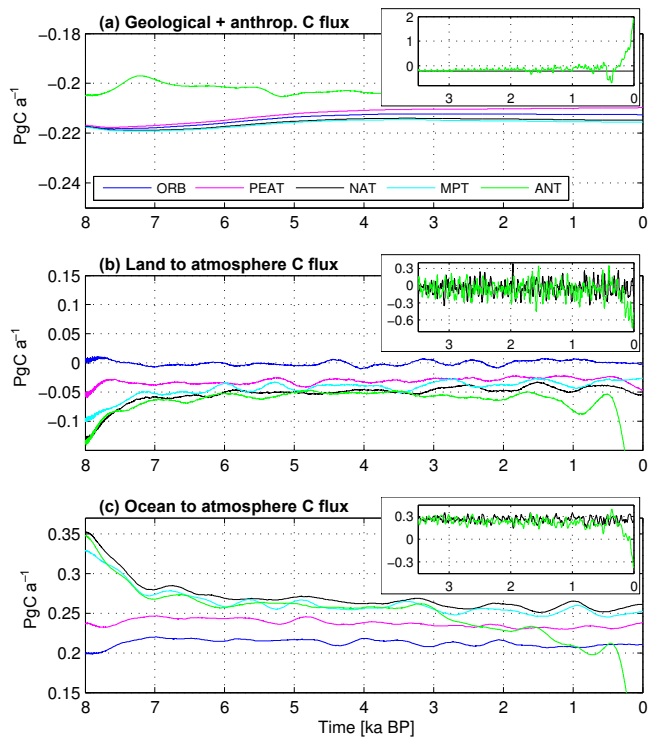


Figure 3. Disaggregation of the net carbon fluxes in the Holocene experiments: geological and anthropogenic flux to atmosphere (a), land–atmosphere flux (b) and ocean–atmosphere flux (c). Plots have been smoothed using a 1000-year Gaussian filter for clarity. Inset figures show fluxes from HOL_ANT and HOL_NAT with axis scaling appropriate for HOL_ANT and smoothed using a 50-year Gaussian filter.

water CaCO_3 accumulation rates (HOL_NAT, HOL_MPT, HOL_ANT, EEM_NAT and MIS11_NAT) sea level changes, and in experiment HOL_ANT anthropogenic CO_2 emissions from land use changes and fossil fuel burning are prescribed, as described in Sect. 2.4.

3 Results

3.1 Holocene

The atmospheric carbon dioxide concentrations resulting from the Holocene experiments are shown in Fig. 2a, as well as ice core data for comparison. In model experiment HOL_ORB (without peat accumulation and CaCO_3 sedimentation in shallow waters), atmospheric CO_2 decreases by ~ 5 ppm over the first 2000 years, followed by constant CO_2 for the remainder of the experiment (Fig. 2a, blue line). In experiment HOL_PEA (which includes carbon accumulation in boreal peatlands but excludes CaCO_3 accumulation in shallow waters), atmospheric CO_2 decreases by 25 ppm from 8 to 0 ka BP (Fig. 2a, magenta line). In experiment HOL_NAT (which includes carbon storage in boreal peatlands and shallow-water CaCO_3 accumulation) atmospheric

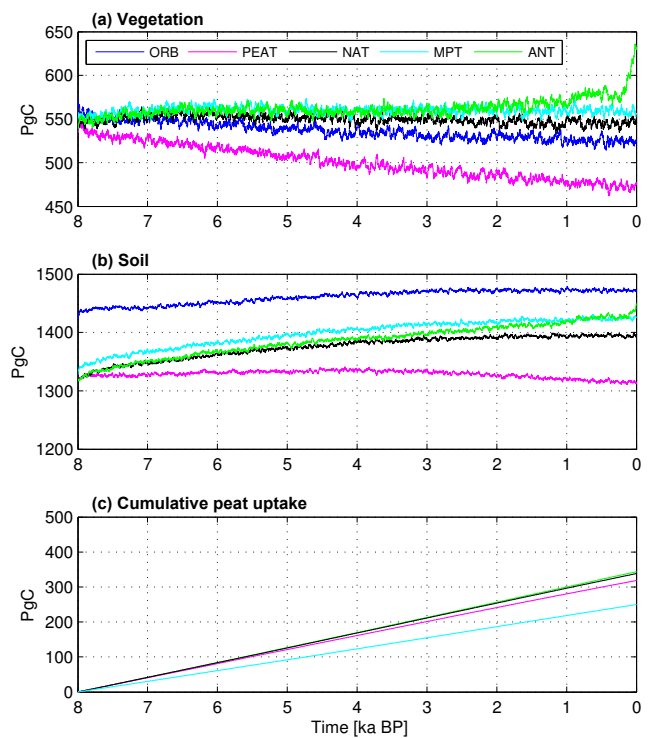


Figure 4. Land carbon pools in Holocene experiments: total vegetation carbon (a), total non-peat soil carbon (b) and cumulative C uptake by peatlands (c).

CO_2 closely follows the ice core measurements until about 3 ka BP (Fig. 2a, black line). Between 8 ka and 6 ka BP, the model overestimates CO_2 by up to 5 ppm, while it underestimates atmospheric CO_2 after 4 ka BP. The discrepancy grows as the model gets closer to the present. Atmospheric CO_2 stays constant at 267 ppm after 4 ka BP in this experiment. In experiment HOL_MPT (as HOL_NAT, but with the minimum peatland area), atmospheric CO_2 increases slightly stronger than in HOL_NAT during the early Holocene and keeps increasing until 2.5 ka BP, after which it stays constant at 273 ppm CO_2 (Fig. 2a, cyan line). Finally, in HOL_ANT (as HOL_NAT but with anthropogenic emissions of CO_2 from land use changes and fossil fuel emissions), the atmospheric CO_2 is similar to CO_2 in HOL_NAT until about 4 ka BP and similar to HOL_MPT until 2.5 ka BP, after which HOL_ANT displays a continued increase in CO_2 , in line with ice core CO_2 (Fig. 2a, green line). The CO_2 trajectory stays relatively close to the measurements over the entire time frame of HOL_ANT.

The disaggregated net carbon fluxes leading to these trajectories in CO_2 are shown in Fig. 3. For clarity we have smoothed the plots using a Gaussian filter (length 1000 a, stronger weighting in the centre following a Gaussian distribution). Fig. 3a shows the geological and anthropogenic C flux to the atmosphere, i.e. the sum of volcanic outgassing, weathering and anthropogenic fluxes, while Fig. 3b shows

the net land–atmosphere carbon flux and Fig. 3c shows the net ocean–atmosphere C flux. Since the volcanic input is constant in time, the changes shown in Fig. 3a mainly reflect changes in weathering, with the exception of experiment HOL_ANT, where the bulk of the changes is due to anthropogenic emissions. In experiment HOL_ORB, shown in blue, weathering takes up slightly more carbon in the early than in the late Holocene. This carbon uptake by weathering is compensated for by C emissions from the ocean, as shown in Fig. 3c, while the land is carbon-neutral. The slight decrease in atmospheric CO₂ displayed during the first 2000 years of experiment HOL_ORB therefore is the result of the slightly stronger weathering during the early Holocene. Although the land is carbon-neutral overall, a shift in carbon allocation becomes apparent in Fig. 4, where the evolutions of the land C pools are shown. In experiment HOL_ORB, vegetation carbon decreases by 30 Pg C over the time of the experiment (Fig. 4a), while soil carbon increases by a similar amount (Fig. 4b).

The decrease in CO₂ in experiment HOL_PEAT (magenta) is caused by an uptake of carbon by the land surface. In Fig. 3b, a more or less constant carbon uptake flux of about $-0.03 \text{ Pg C a}^{-1}$ is shown, caused by the accumulation of 310 Pg C of peat (Fig. 4c). Vegetation loses about 80 Pg C (Fig. 4a), while soils lose about 20 Pg C (Fig. 4b), due to the lower concentration of atmospheric CO₂, lessening the impact of the peat accumulation. Note that the overall soil C pool is decreased in comparison to HOL_ORB for all experiments considering peat carbon accumulation since the area available for carbon storage in mineral soils is decreased due to the consideration of peatlands. In addition, C is released from the ocean (Fig. 3c), partially compensating for the carbon uptake.

Carbon fluxes in experiments HOL_NAT and HOL_MPT are very similar. They also display a slight decrease in the atmospheric weathering flux (Fig. 3a), though less pronounced than in experiments HOL_ORB and HOL_PEAT due to the higher concentration in atmospheric CO₂ later in the Holocene. The uptake of carbon by the land, shown in Fig. 3b, is higher than in experiment HOL_PEAT, due to higher CO₂ concentrations, and displays a maximum at the beginning of the experiment. Soil carbon (Fig. 4b) increases over the entire experiment, while vegetation carbon (Fig. 4a) stays constant. Peat accumulates (Fig. 4c) in both experiments, though the total accumulation is different: 340 Pg C in HOL_NAT but only 250 Pg C in HOL_MPT. The increase in atmospheric CO₂ during the early Holocene is driven by the release of carbon from the ocean in these experiments, as shown in Fig. 3c. This increase in C release from the ocean relative to the previous experiments is caused by the release of CO₂ during the formation of the CaCO₃ that accumulates in shallow waters, especially in coral reefs, as shown in Fig. 5b. The coral CaCO₃ accumulation flux is 28 Tmol a^{-1} during the early Holocene due to the large change in sea level

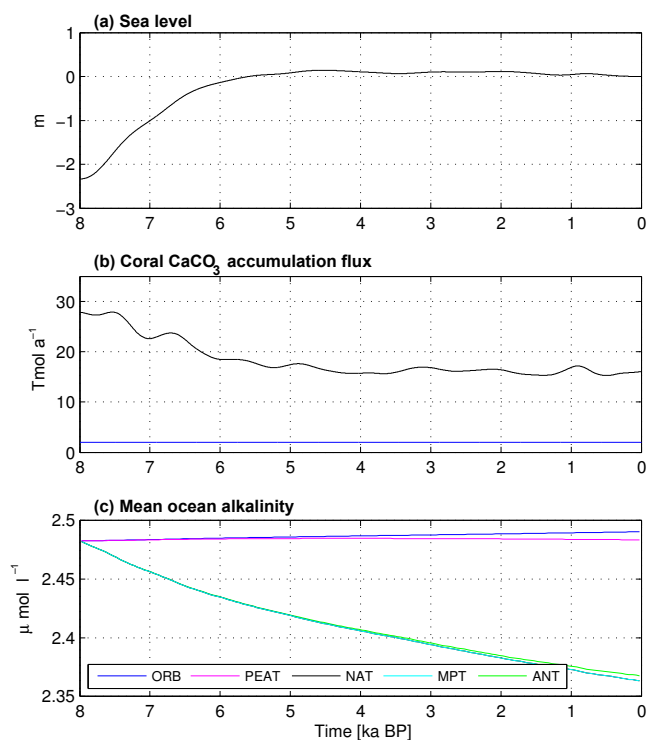


Figure 5. Sea level forcing (a), shallow-water CaCO₃ accumulation flux (b) and mean ocean alkalinity (c) in the Holocene experiments. Plots have been smoothed for clarity.

(Fig. 5a). It decreases to 18 Tmol a^{-1} at 4 ka BP and stays constant thereafter due to the constant sea level.

Carbon fluxes in experiment HOL_ANT cannot be shown fully in Fig. 3 since their magnitude becomes substantially larger than the natural carbon fluxes described for the previous experiments towards the late Holocene. We have therefore added inset figures showing fluxes from HOL_NAT and HOL_ANT for the last 3.5 kyr of the experiments. The plots in the inset figures have been smoothed using a shorter filter length of 50 years since the long filtering used previously hides the substantial changes induced by industrial CO₂ emissions after AD 1765. The geological and anthropogenic C flux to the atmosphere peaks at 2 Pg C a^{-1} in 0 BP, due to the large anthropogenic C emissions. During the early Holocene the anthropogenic flux is substantially smaller though. Here, it lessens the impact of weathering and slightly increases the geological and anthropogenic C flux to the atmosphere in comparison to HOL_NAT, as shown in Fig. 3a. The land–atmosphere flux is very similar to experiment HOL_NAT until 3 ka BP; the land generally takes up carbon due to peat accumulation. After 3 ka BP, the land–atmosphere flux becomes more negative than in the other experiments; the land C uptake increases due to CO₂ fertilization and reaches a minimum of -0.6 Pg C a^{-1} at the end of the experiment (Fig. 3b, inset figure). This is reflected in the land C pools (Fig. 4), which keep increasing through-

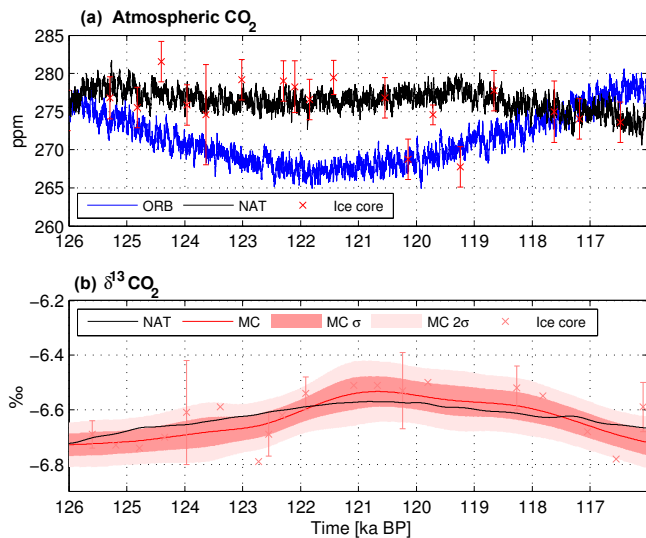


Figure 6. Eemian CO₂ concentration (a) and δ¹³CO₂ (b) from model experiments and ice core data. δ¹³CO₂ model results have been smoothed for clarity and offset, as described in the text. Ice core CO₂ data are from EDC as compiled by Bereiter et al. (2015). δ¹³CO₂ data are from EDC (Schneider et al., 2013), with Monte Carlo average (MC) and uncertainty estimate (MC σ).

out experiment HOL_ANT. The ocean–atmosphere flux in experiment HOL_ANT is similar to those in experiments HOL_NAT and HOL_MPT, though slightly smaller, until 3 ka BP, when it starts deviating from the other experiments (Fig. 3c). The flux becomes negative after 75 BP (AD 1875; Fig. 3c, inset figure); i.e. the ocean switches from being a sink for carbon to a source.

The increase in atmospheric CO₂ during the early Holocene in experiments HOL_NAT, HOL_MPT and HOL_ANT is due to the strongly positive ocean–atmosphere carbon flux, caused by the accumulation of CaCO₃ in shallow waters. Sea level initially rises fast (see Fig. 5a), reaching stable levels around 5 ka BP. The shallow-water CaCO₃ accumulation rate, shown in Fig. 5b, varies with the rate of sea level change. The rate of sea level change is highest early during the Holocene (about 2 mm a⁻¹), leading to a CaCO₃ accumulation of about 27 Tmol a⁻¹. Sea level stabilizes later in the Holocene, reducing shallow-water CaCO₃ accumulation to about 15 Tmol a⁻¹ in all three experiments. The formation of CaCO₃ in experiments HOL_NAT, HOL_MPT and HOL_ANT leads to a reduction in mean ocean alkalinity, as shown in Fig. 5c. Over the course of the Holocene, the mean ocean alkalinity is reduced by about 10 % in the experiments where shallow-water CaCO₃ accumulation is considered.

The evolution of atmospheric δ¹³CO₂ in experiments HOL_NAT, HOL_MPT and HOL_ANT is shown in Fig. 2b. The plots are smoothed using a Gaussian filter for clarity. To enable comparison of the trends in δ¹³CO₂ to ice core data, we also added a small constant offset to

these results (−0.0712 ‰ for HOL_NAT and HOL_ANT, and −0.04 ‰ for HOL_MPT). This offset became necessary because the model displays a small drift in δ¹³CO₂ when coupling the interactive CO₂ from CLIMBER and the LPJ land carbon cycle after the spin-up of LPJ. Modelled δ¹³CO₂ increases from −6.4 to −6.2 ‰ for experiments HOL_NAT and HOL_MPT, while HOL_ANT displays an increase from −6.4 to −6.3 ‰ at 3 ka BP and decreases again thereafter. The Schmitt et al. (2012) Monte Carlo average of δ¹³CO₂ increases from −6.4 to −6.33 ‰ at 6 ka BP and slowly decreases again thereafter. The model trajectories from HOL_NAT and HOL_MPT stay within the 1σ Monte Carlo uncertainty range until 4.8 ka BP and leave the 2σ uncertainty range after 3.9 ka BP. For experiment HOL_ANT, the trajectory of δ¹³CO₂ stays within the 2σ uncertainty range for the entire experiment. Considering the measurement data directly, as shown by the error bars in Fig. 2b, the trajectories from experiments HOL_NAT and HOL_MPT leave the range of the error bars at 2.5 ka BP, while HOL_ANT remains within the range of the error bars for most of the measurements until the end of the experiment.

3.2 Eemian

The CO₂ concentrations from the Eemian experiments EEM_ORB and EEM_NAT are shown in Fig. 6a, together with the ice core data. Experiment EEM_ORB (blue line), is in poor agreement with the ice core data. CO₂ decreases from the initial value of 276 to about 267 ppm CO₂ at 121 ka BP, after which it increases again to 278 ppm at 116 ka BP. In experiment EEM_NAT, in contrast, modelled atmospheric CO₂ changes relatively little for the entire experiment and is generally within the range spanned by the error bars of the measurements, with exceptions only around 119.5 ka BP, where three data points show lower CO₂ concentrations than modelled. δ¹³CO₂ for EEM_NAT, smoothed by a Gaussian filter and offset by −0.0647 ‰ as for the Holocene experiments, is shown in Fig. 6b. Modelled δ¹³CO₂ stays within the 1σ uncertainty of the Monte Carlo estimate from Scheider et al. (2013) for the entire time of the experiment.

The disaggregated net carbon fluxes leading to these CO₂ trajectories are shown in Fig. 7. Weathering is very strong during the early Eemian, leading to a geological C flux of −0.24 Pg C a⁻¹ for 126 ka BP, shown in Fig. 7a. Weathering then decreases, allowing the geological C flux to increase to −0.205 Pg C a⁻¹ at 116 ka BP in both experiments. While the geological C flux is similar in both experiments, the other C fluxes are substantially different. For experiment EEM_ORB, the land is generally carbon-neutral during the early Eemian. The land–atmosphere C flux is close to zero until 121.5 ka BP (see Fig. 7b). Later in the Eemian, the land–atmosphere C flux increases to a maximum of 0.05 Pg C a⁻¹ at 117 ka BP. For the early Eemian this is due to counteracting contributions from the land carbon pools: vegetation carbon decreases continually from 126 to 116 ka BP,

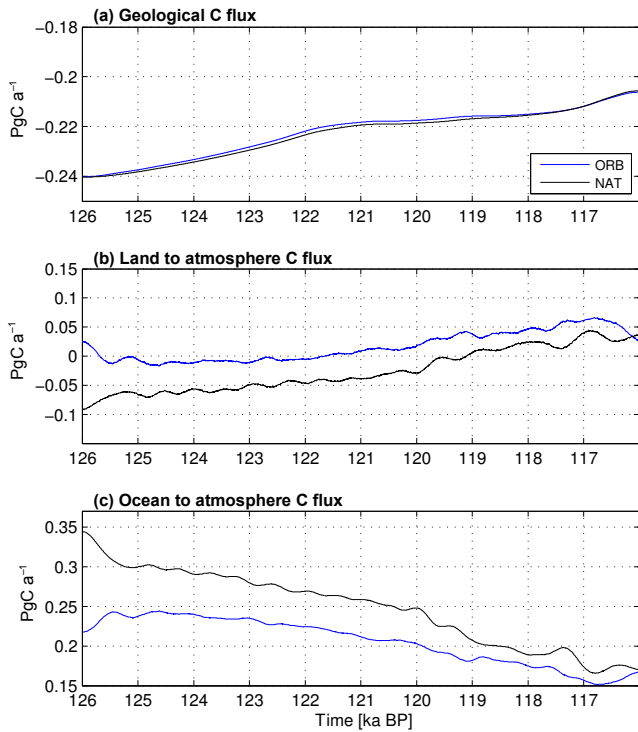


Figure 7. Disaggregation of the net carbon fluxes in the Eemian experiments: geological flux to atmosphere (a), land–atmosphere flux (b) and ocean–atmosphere flux (c). Plots have been smoothed for clarity.

with an initially slow rate of decrease that increases after 123 ka BP (see Fig. 8a). Soil carbon, in contrast, increases from 1415 Pg C at 126 ka BP to 1480 Pg C at 120.5 ka BP, after which it decreases to 1350 Pg C at 116 ka BP (Fig. 8b). The ocean–atmosphere carbon flux, on the other hand, is initially at 0.23 Pg C a^{-1} and decreases to a minimum of 0.15 Pg C a^{-1} at 117 ka BP. Therefore, the initial strong carbon uptake through weathering is not completely compensated for by marine C fluxes, leading to the modelled reduction in atmospheric CO_2 between 126 and 121.5 ka BP. After this time, the land loses carbon, allowing a compensation of the (reduced) weathering flux and leading to an increase in atmospheric CO_2 .

In experiment EEM_NAT, on the other hand, the land–atmosphere C flux is negative until 119.5 ka BP, increasing from $-0.095 \text{ Pg C a}^{-1}$ at 126 ka BP to 0.04 Pg C a^{-1} at 116 ka (Fig. 7b). While the vegetation and soil carbon pools behave in a generally similar way to experiment EEM_ORB (Fig. 8a, b), the model accumulates 445 Pg C of peat carbon (Fig. 8c), resulting in the generally negative land–atmosphere flux. The ocean–atmosphere flux initially is substantially higher than in EEM_ORB, with an initial flux of 0.33 Pg C a^{-1} , that decreases over time to 0.17 Pg C a^{-1} . The sea level, shown in Fig. 9a, is stable early during the experiment and decreases after 121 ka BP. Therefore, shallow-

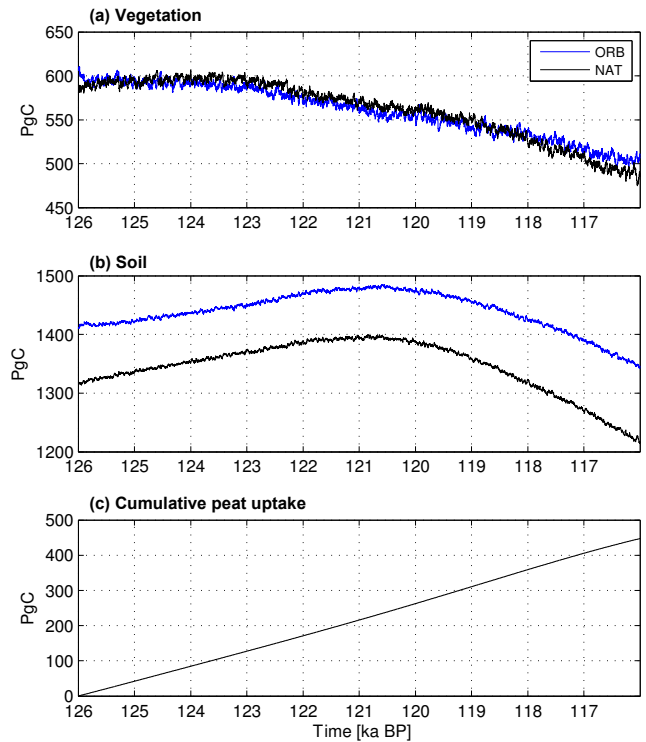


Figure 8. Land carbon pools in the Eemian experiments: total vegetation carbon (a), total non-peat soil carbon (b) and cumulative C uptake by peatlands (c).

water CaCO_3 accumulates at a rate of $\sim 20 \text{ Tmol a}^{-1}$ during the early Eemian (Fig. 9b), lower than during the early Holocene. It decreases to about zero at 119 ka and stays at this level thereafter. This increases the ocean–atmosphere flux in comparison to experiment EEM_ORB, thus releasing carbon to the atmosphere, which compensates for the peat carbon uptake and the strong weathering flux during the early Eemian.

3.3 MIS 11

For MIS 11, the agreement between the modelled atmospheric CO_2 concentrations in MIS11_NAT and the ice core reconstruction is not as good as for the other two interglacials. As shown in Fig. 10, modelled CO_2 in experiment MIS11_NAT increases initially from 271 ppm CO_2 to about 290 ppm at 412 ka BP. It declines thereafter to about 250 ppm CO_2 at 395 ka BP, after which CO_2 varies much less. Set-up MIS11_ORB, on the other hand, shows a slowly decreasing trend in CO_2 , from the initial 271 ppm CO_2 to slightly less than 260 ppm at 380 ka BP, with only little variation about this trend.

The initial increase in CO_2 is slower in the ice core data than in MIS11_NAT. CO_2 increases to about 285 ppm at 407 ka BP. Measured CO_2 decreases strongly after 398 ka BP, until 250 ppm CO_2 is reached at 390 ka BP. Therefore, the

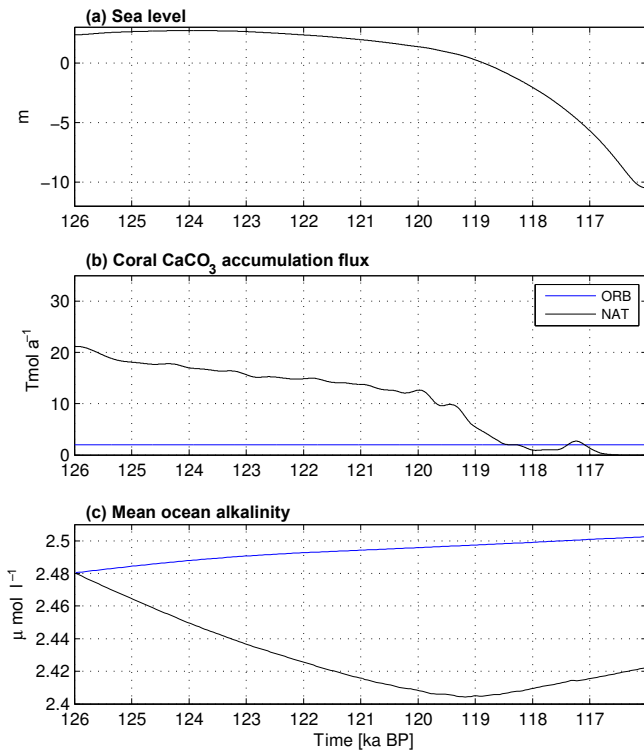


Figure 9. Sea level forcing (a), shallow-water CaCO_3 accumulation flux (b) and mean ocean alkalinity (c) in the Eemian experiments. Plots have been smoothed for clarity.

model set-up MIS11_NAT overestimates the initial increase in CO_2 , and the peak in CO_2 is reached about 5 kyr earlier than in the ice core data. Similarly, the decrease after the peak in CO_2 also occurs earlier in the model than in the ice core data. Nonetheless, the overall CO_2 trajectory, with an initial increase in CO_2 between 420 ka and 405 ka BP, followed by a decrease by about 25–30 ppm and a stabilization of CO_2 after 395 ka BP is captured by MIS11_NAT, though the timing is not exactly the same as in the ice core data. MIS11_ORB, on the other hand, does not at all follow the ice core CO_2 data. For the interested reader, we show the $\delta^{13}\text{CO}_2$ for experiment MIS11_NAT in Fig. 10b, though no ice core data are available for comparison. $\delta^{13}\text{CO}_2$ starts out at -6.5‰ , with a slowly decreasing trend until 405 ka BP. Afterwards it decreases quickly to -6.55‰ at 398 ka BP. It then slightly increases again until 390 ka BP, after which it decreases further until -6.57‰ is reached at 380 ka BP.

The geological C flux, shown in Fig. 11a, is very similar in both experiments; changes in MIS11_NAT only present a slightly larger amplitude than MIS11_ORB due to the higher CO_2 concentrations. It decreases from $-0.208 \text{ Pg C a}^{-1}$ at 420 ka BP to $-0.233 \text{ Pg C a}^{-1}$ at 410 ka BP in MIS11_NAT, reflecting increases in weathering. Subsequently it increases to the initial value at 395 ka BP, followed by a small decrease and further increase to a final value of $-0.204 \text{ Pg C a}^{-1}$.

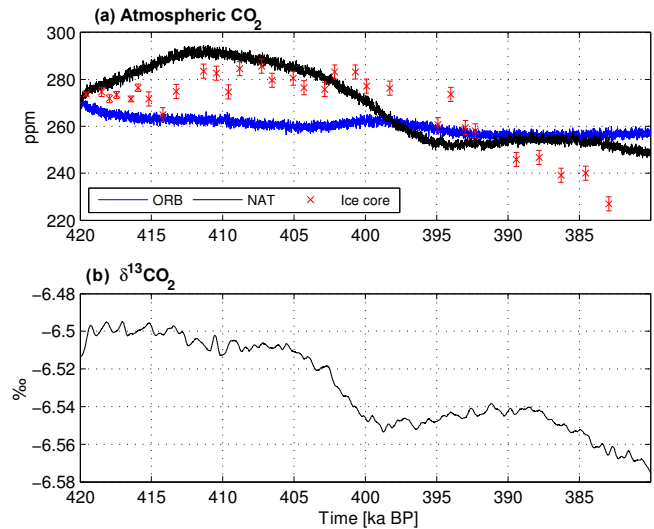


Figure 10. MIS 11 CO_2 concentration (a) from model experiments and ice core data, and $\delta^{13}\text{CO}_2$ of CO_2 from model experiment MIS11_NAT. $\delta^{13}\text{CO}_2$ model results have been smoothed for clarity. Ice core CO_2 data are from EDC and Vostok as compiled by Bereiter et al. (2015). $\delta^{13}\text{CO}_2$ from ice cores is not available.

The land–atmosphere flux in experiment MIS11_ORB fluctuates around zero (Fig. 11b), with increases in vegetation carbon (Fig. 12a) compensated for by decreases in soil carbon (Fig. 12b) and vice versa. In MIS11_NAT, the net land–atmosphere flux is more negative due to the accumulation of peat carbon. It is $-0.09 \text{ Pg C a}^{-1}$ initially and increases to zero at 400 ka BP, with a subsequent decrease to $-0.035 \text{ Pg C a}^{-1}$ at 395 ka BP and an increase to $-0.01 \text{ Pg C a}^{-1}$ at 380 ka BP. This is due to the changes in the land carbon pools: vegetation carbon (Fig. 11a) increases strongly, until a maximum value of about 630 Pg C is reached at 412 ka BP. Carbon storage decreases afterwards, until a minimum of 480 Pg C is reached at 395 ka BP, with only small changes afterwards. Similarly, soil carbon increases early in MIS11_NAT from an initial value of 1350 to about 1425 Pg C at 414 ka BP. It then stays constant until 403 ka BP, when it starts to strongly decrease. After 395 ka BP soil carbon stays constant at 1345 Pg C. Peat accumulation in MIS11_NAT (Fig. 11c) increases nearly linearly between 420 and 398 ka BP. After 398 ka BP the rate of increase decreases slightly due to the lower atmospheric CO_2 concentration.

The net ocean–atmosphere flux, shown in Fig. 11c, is nearly constant at 0.21 Pg C a^{-1} in experiment MIS11_ORB. In experiment MIS11_NAT, on the other hand, the flux is initially at $0.313 \text{ Pg C a}^{-1}$, then decreases to about $0.207 \text{ Pg C a}^{-1}$ at 400 ka BP, to increase to $0.273 \text{ Pg C a}^{-1}$ over the next 10 kyr. These changes in the ocean–atmosphere C flux are mainly driven by changes in the CaCO_3 accumulation in shallow waters. During the first 13 kyr of MIS 11, sea level increases from -20 m to near zero (Fig. 12a). It then

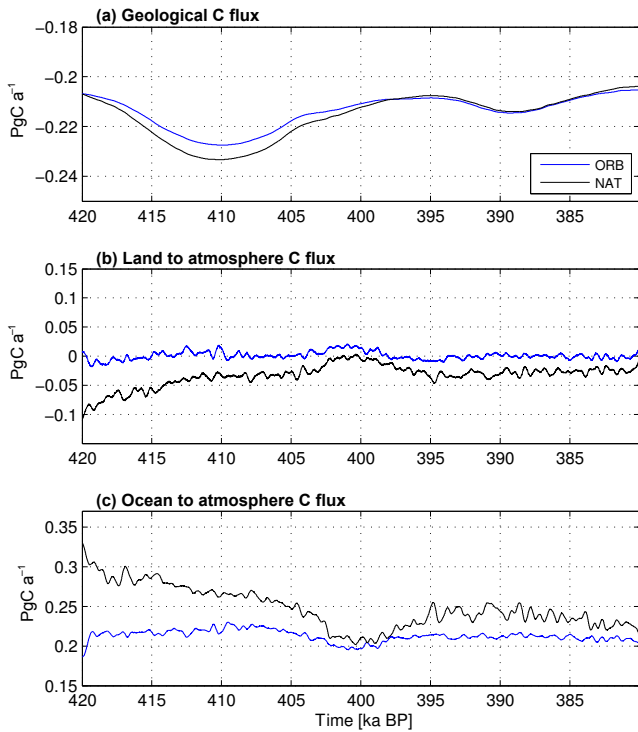


Figure 11. Disaggregation of the net carbon fluxes in the MIS 11 experiments: geological flux to atmosphere (a), land–atmosphere flux (b) and ocean–atmosphere flux (c). Plots have been smoothed for clarity.

decreases again at 407 ka BP but stabilizes at -15 m after 395 ka BP. This sea level trajectory is reflected in the CaCO_3 accumulation flux, shown in Fig. 12b: the initial fast rise in sea level leads to an accumulation rate of up to 29 Tmol a^{-1} , with a correspondingly high CO_2 release to the atmosphere, which declines between 413 and 400 ka BP, when the accumulation rate is zero due to the decrease in sea level. With the slowing rate of sea level decrease, sedimentation increases again after 396 ka BP and reaches values of about 15 Tmol a^{-1} again at 390 ka BP.

4 Discussion

From our results for the Holocene carbon cycle, it becomes quite clear that all of the forcings and processes considered taken together deliver the best match to the ice core CO_2 data. The model set-up HOL_ORB, i.e. a carbon cycle set-up without anthropogenic CO_2 emissions nor slow natural processes, leads to a more or less constant CO_2 trajectory, where the carbon uptake by weathering is compensated for by a carbon release from the ocean, while the land is generally carbon-neutral. The consideration of peat accumulation by itself in HOL_PEAT leads to a decrease in atmospheric carbon dioxide due to a large carbon uptake by the land, which is partially compensated for by additional carbon release from the ocean,

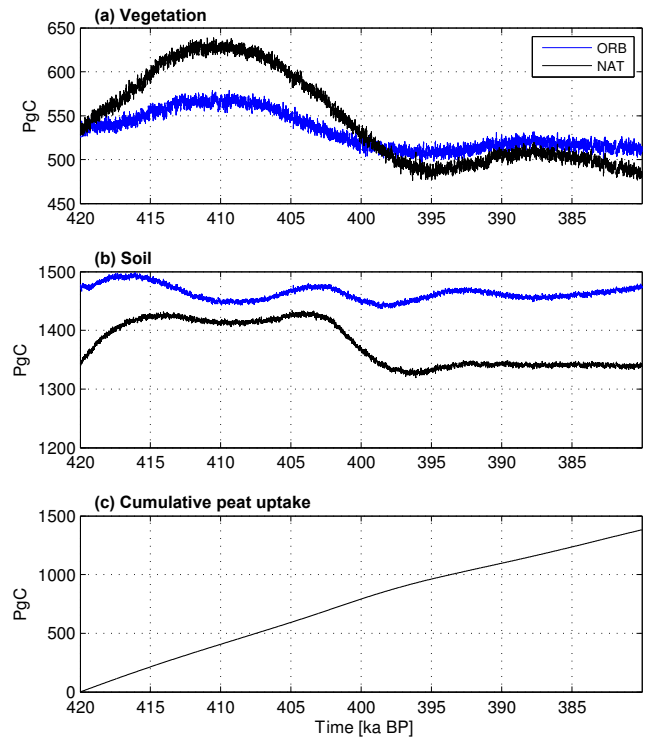


Figure 12. Land carbon pools in the MIS 11 experiments: total vegetation carbon (a), total non-peat soil carbon (b) and cumulative C uptake by peatlands (c).

in comparison to HOL_ORB. The additional consideration of CO_2 emissions from CaCO_3 shallow-water sedimentation in HOL_NAT then leads to an increase in atmospheric CO_2 , not just compensating for the C uptake by peatlands but also releasing additional CO_2 to the atmosphere.

According to the “early anthropogenic hypothesis” (Rudiman, 2003, 2013), anthropogenic emissions related to land use from early agriculture strongly influenced climate already in the early Holocene. The present study does not aim at either validating or falsifying this hypothesis. However, it becomes clear from the difference between experiments HOL_NAT and HOL_ANT that anthropogenic CO_2 emissions from land use changes only make a significant difference to atmospheric CO_2 after about 3 ka BP, which would shift to an even later time with smaller peat carbon accumulation (as in HOL_MPT). Anthropogenic emissions therefore cannot explain the 10 ppm rise in CO_2 observed in ice cores between 8 and 4 ka BP. For the earlier Holocene, CO_2 emissions from shallow-water CaCO_3 sedimentation are required instead. The continued rise in CO_2 after 2.5 ka BP, on the other hand, can only be explained if anthropogenic emissions are accounted for as well.

Our assessment contains several uncertainties. The modelled peat accumulation rates compare well to site data (Kleinen et al., 2012), and the overall peatland carbon accumulation fits in well with observed peat carbon stocks (Yu

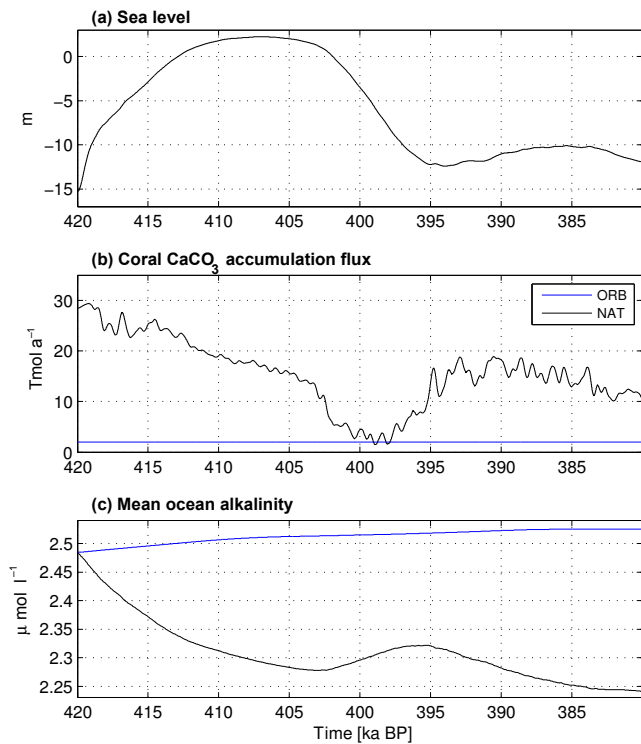


Figure 13. Sea level forcing (a), shallow-water CaCO_3 accumulation flux (b) and mean ocean alkalinity (c) in the MIS 11 experiments. Plots have been smoothed for clarity.

et al., 2010), which are relatively well constrained. What is less well constrained is the peatland carbon accumulation history, and our modelled peatland carbon accumulation trajectory may not reflect the actual accumulation history. What is also not very well constrained is the areal extent of peatlands (Kleinen et al., 2012), as well as its temporal development. MacDonald et al. (2006) and Yu et al. (2010) show high rates of peatland initiation between 11 and 9 ka BP, possibly caused by the high northern, high-latitude insolation during this time. Northern peatland initiation dates decrease in number after this time but remain significant. In our model peatland area changes little after 8 ka BP, one of the reasons for the nearly linear accumulation of carbon in peatlands. We also neglect the small remains of the Laurentide ice sheet remaining at 8 ka BP, since we have shown that its influence is small (Kleinen et al., 2012). The change in peatland area over the time of the model simulation may therefore be underestimated by our model, which would modify the trajectory of peat carbon accumulation to a trajectory where less carbon is accumulated earlier in the Holocene and more C is accumulated later.

Modelled vegetation changes in our model compare well to tree cover reconstructions from Eurasia (Kleinen et al., 2011). They are also similar to vegetation changes obtained with other models, for example CLIMBA and Bern3D, as

published by Brovkin et al. (2016). However, it is not possible to validate the modelled changes in terrestrial carbon storage since no direct proxy exists for carbon stored in terrestrial ecosystems. The CO_2 fertilization effect displayed by CLIMBER2-LPJ as well as other DGVMs, which leads to increases in biomass with increasing CO_2 , seems well understood at the leaf level (De Kauwe et al., 2014) but may be overestimated in models because constraining mechanisms such as nutrient limitation are not taken into account (Reich et al., 2014).

Our CaCO_3 accumulation model seems to capture the late Holocene sedimentation, in good agreement with Milliman (1993). Nonetheless the increase in accumulation rate due to the rate of sea level rise during the earlier Holocene is relatively uncertain. This is due to uncertainties in the parameterization, as well as uncertainties in the rate of sea level rise. While both are plausible, there is considerable uncertainty with respect to magnitude and timing of the CO_2 emissions from CaCO_3 formation. Previous assessments nevertheless agree that coral growth was stronger in the early Holocene (Ryan et al., 2001; Vecsei and Berger, 2004). The change in sea level we use as a model forcing agrees well with sea level reconstructions for the Holocene, though sea level stabilizes up to 2 kyr earlier in our model than it does in reconstructions (Masson-Delmotte et al., 2013, Fig. 5.17f). A later stabilization of the sea level, as in palaeoclimatic archives, would lead to a prolongation of the relatively larger emissions from CaCO_3 formation we model for the early Holocene. Therefore, we may underestimate the emissions from shallow-water CaCO_3 accumulation.

Finally, the modelled trajectory of $\delta^{13}\text{C}$ for the Holocene stays well within the 2σ uncertainty band of the Monte Carlo-based uncertainty assessment by Schmitt et al. (2012) if one considers experiment HOL_ANT, while the other experiments leave this range. While the general dynamics of ^{13}C seem to be captured well by the LPJ model (Scholze et al., 2003), there is some uncertainty with regard to the ^{13}C changes induced by the accumulation of peat. We assume that the carbon uptake by peat accumulation has a similar signature in $\delta^{13}\text{C}$ as the growth of C3 grass. Since photosynthesis in mosses generally follows the C3 pathway, this assumption appears reasonable, and values for $\delta^{13}\text{C}$ in mosses reported in the literature are in a similar range as values for other C3 vegetation (e.g. Waite and Sack, 2011). However, the cycling of ^{13}C in peatlands seems to be less well understood than in other terrestrial systems, which makes the modelled $\delta^{13}\text{C}$ changes induced by peat accumulation less certain. In addition we cannot rule out other isotopically depleted sources of C, such as methane emissions or the release of carbon from thawing permafrost soils, that we have not accounted for in our model.

With regard to the evolution of atmospheric CO_2 during the Eemian, the fit between ice core data and model results is clearly better for experiment EEM_NAT than for EEM_ORB. While the model produces an initial decrease

followed by an increase for EEM_ORB, EEM_NAT shows a nearly constant CO₂ concentration for the entire period of time we modelled, very close to the measurements from Bereiter et al. (2015). Similarly, modelled $\delta^{13}\text{C}_{\text{CO}_2}$ is within the 1σ uncertainty range of the Schneider et al. (2013) Monte Carlo average for most of the time, though the model displays less change in $\delta^{13}\text{C}_{\text{CO}_2}$ than the MC average. Here the largest uncertainty in our set-up again stems from the sea level history, leading to uncertainty with respect to magnitude and timing of CO₂ emissions that result from CaCO₃ sedimentation. However, the sea level forcing we use is similar to reconstructed global mean sea level as shown by Masson-Delmotte et al. (2013, Fig. 5.15a and b) and should therefore be a reasonable approximation. In our set-up, and with the sea level forcing data we use, the CO₂ emissions from CaCO₃ sedimentation counterbalance the weathering-induced decrease in CO₂ shown in set-up EEM_ORB for the early Eemian, while carbon uptake by peatlands compensates for the increase in CO₂ modelled in EEM_ORB during the second half of the Eemian.

For MIS 11 our model experiment MIS11_NAT displays a qualitatively similar evolution of atmospheric CO₂ as the ice core data, with an initial increase, followed by a decrease during the middle of the interglacial until the CO₂ concentration stabilizes for the later part of the interglacial. This leads to a clearly better fit to the ice core measurements than set-up MIS11_ORB, which shows a continuous slow decrease of atmospheric CO₂. Nonetheless there still are discrepancies in the timing and the magnitude of the changes in CO₂ between model and ice core data. This discrepancy is most likely again due to uncertainty in the sea level history that we use to force the model. Sea level reconstructions for MIS11 show considerable discrepancies between each other, making an evaluation of the quality of our forcing data very difficult. Between the four reconstructions of MIS11 sea level that we considered (Waelbroeck et al., 2002; Rohling et al., 2010; Elderfield et al., 2012; Grant et al., 2014), there is a general qualitative agreement in timing: sea level rises between 420 and 405 ka BP, followed by a decrease. While the sea level history from Waelbroeck et al. (2002) shows a sustained decrease, this decrease ends at about 390 ka BP in the other three reconstructions, followed by either a plateau or a slight increase. The four reconstructions furthermore disagree with regard to the magnitude of changes, with the sea level highstand at ~ 405 ka BP ranging from -10 to $+30$ m relative to the present. Our forcing trajectory falls well within the range of these reconstructions. However, the magnitude and timing of changes in sea level have a large impact on the CO₂ emissions from shallow-water CaCO₃ accumulation, making the latter relatively uncertain. If, for example, the increase in sea level before 410 ka BP were slightly less pronounced in our forcing data and the decrease in sea level after 405 ka BP slightly delayed, our model results would better fit the ice core data.

Our study has several other limitations. We imposed anthropogenic emissions from land use changes as a simple flux to the atmosphere without changing the land carbon stocks. This simplification modifies the uptake of carbon by the biosphere and should already be contained in the Kaplan et al. (2011) CO₂ emission estimate, but an inconsistency remains nonetheless. We also neglected the long-term memory of the carbonate compensation response to the release of carbon from the deep ocean and the early interglacial carbon uptake by the terrestrial biosphere during deglaciation. While CLIMBER2-LPJ contains all relevant processes, we did not model this period transiently and our results therefore do not contain the long-term memory signal. Menviel and Joos (2012) found that these memory effects could be of the order of a few ppm for the Holocene. We furthermore assumed that the long-term carbon cycle was in equilibrium in the pre-industrial climate, but this assumption is a simplification as the balance between carbonate burial, weathering and volcanic outgassing could be out of equilibrium for other climates. As follows from control simulations without forcings (not shown), these effects can be of the order of few parts per million as well. Furthermore, the zonally averaged ocean model in CLIMBER2 may underestimate short-term variability in ocean circulation and export production. This was not the focus of our study and should not be relevant for the millennial-scale evolution of the carbon cycle investigated here. However, an impact cannot be excluded. Last, but not least, several other mechanisms that are currently under discussion such as changes in permafrost carbon pools (Schneider von Deimling et al., 2012) or methane hydrate storages (Archer et al., 2009) are not accounted for, as modelling of these processes is still at an early stage and because of the lack of reliable constraints on the amplitude of interglacial changes in these potentially large carbon pools.

5 Conclusions

We show – to the best of our knowledge for the first time – how the trends in interglacial atmospheric CO₂, as reconstructed from ice cores, can be reproduced relatively well by a climate model with identical forcing parameterization for three recent interglacials. These trends in atmospheric CO₂ cannot be reproduced well if only the marine and terrestrial carbon cycle components, as implemented in most Earth system models (Ciais et al., 2013), are considered. Instead, the modelled CO₂ change is considerably improved if two slow processes of CO₂ change currently neglected in the most comprehensive carbon cycle models, namely the carbon accumulation in peatlands and the CO₂ release from CaCO₃ accumulation in shallow waters, are accounted for as well. The latter process leads to an increase in atmospheric CO₂ during periods of constant or slowly rising sea level, while the former process leads to a decrease in atmospheric CO₂.

For the Holocene, we can explain the rise in atmospheric CO₂ between 8 ka BP and 3 ka BP purely by natural forcings, while later in the Holocene, starting at about 3 ka BP, anthropogenic emissions from land use changes and fossil fuel use play an important role. The increase in atmospheric CO₂ during the early Holocene therefore is the result of enhanced shallow-water accumulation of CaCO₃ due to rising sea level. For the Eemian, our model also yields an atmospheric CO₂ history that is in close agreement with the ice core data. Here the consideration of the slow carbon cycle processes also leads to an improvement over the conventional model approach that neglects these. For MIS 11, finally, the conventional model set-up does not produce the changes in CO₂ observed throughout MIS 11, while the model with consideration of the slow forcings can explain the magnitude of changes in atmospheric CO₂, though the timing of changes is slightly different from the ice core data. This discrepancy is possibly due to the sea level forcing history that we use to drive the shallow-water CaCO₃ accumulation in our model and which remains uncertain.

Despite the uncertainties discussed above, we can draw some robust conclusions with regard to the timing of CO₂ changes. Early during interglacials, when sea level still rises, shallow-water accumulation of CaCO₃ and the related CO₂ release is larger than in periods of stagnating or receding sea level. The carbon uptake by peatlands, on the other hand, is a more or less constant forcing factor. This uptake balances the CO₂ emission from CaCO₃ precipitation during periods of constant sea level. A rising sea level therefore leads to atmospheric CO₂ increases, while a decline in sea level strongly reduces shallow-water CaCO₃ accumulation, leading to a reduction in atmospheric CO₂.

6 Data availability

Due to licensing constraints, model code cannot be made publically available. However, the model code, primary data, secondary data, and scripts that may be useful in reproducing the authors' work are archived by the Max Planck Institute for Meteorology. They can be made available by contacting the first author or publications@mpimet.mpg.de.

Acknowledgements. Thomas Kleinen acknowledges support through the DFG (Deutsche Forschungsgemeinschaft) priority research program INTERDYNAMIK. Guy Munhoven is a Research Associate with the Belgian Fonds de la Recherche Scientifique – FNRS. We thank Andrey Ganopolski for providing the sea level forcing and Katharina Six for providing valuable comments on an earlier version of this paper. We also thank Dallas Murphy and Jochem Marotzke, as well as the participants of the scientific writing workshop at the MPI for Meteorology, whose comments on style led to substantial improvements of the present text. We finally thank two anonymous reviewers for their constructive input.

The article processing charges for this open-access

publication were covered by the Max Planck Society.

Edited by: L. Skinner

Reviewed by: two anonymous referees

References

- Archer, D. E.: Modeling the calcite lysocline, *J. Geophys. Res.*, 96, 17037–17050, 1991.
- Archer, D., Buffett, B., and Brovkin, V.: Ocean methane hydrates as a slow tipping point in the global carbon cycle, *P. Natl. Acad. Sci. USA*, 106, 20596–20601, doi:10.1073/pnas.0800885105, 2009.
- Bazin, L., Landais, A., Lemieux-Dudon, B., Toyé Mahamadou Kele, H., Veres, D., Parrenin, F., Martinerie, P., Ritz, C., Capron, E., Lipenkov, V., Loutre, M.-F., Raynaud, D., Vinther, B., Svensson, A., Rasmussen, S. O., Severi, M., Blunier, T., Leuenberger, M., Fischer, H., Masson-Delmotte, V., Chappellaz, J., and Wolff, E.: An optimized multi-proxy, multi-site Antarctic ice and gas orbital chronology (AICC2012): 120–800 ka, *Clim. Past*, 9, 1715–1731, doi:10.5194/cp-9-1715-2013, 2013.
- Berger, A.: Long-term variations of daily insolation and Quaternary climatic changes, *J. Atmos. Sci.*, 35, 2362–2367, 1978.
- Bereiter, B., Eggleston, S., Schmitt, J., Nehrbass-Ahles, C., Stocker, T. F., Fischer, H., Kipfstuhl, S., and Chappellaz, J.: Revision of the EPICA Dome C CO₂ record from 800 to 600 kyr before present, *Geophys. Res. Lett.*, 42, 542–549, doi:10.1002/2014GL061957, 2015.
- Brovkin, V., Bendtsen, J., Claussen, M., Ganopolski, A., Kutzbach, C., Petoukhov, V., and Andreev, A.: Carbon cycle, vegetation, and climate dynamics in the Holocene: experiments with the CLIMBER-2 model, *Global Biogeochem. Cy.*, 16, 1139, doi:10.1029/2001GB001662, 2002.
- Brovkin, V., Ganopolski, A., Archer, D., and Rahmstorf, S.: Lowering of glacial atmospheric CO₂ in response to changes in oceanic circulation and marine biogeochemistry, *Paleoceanography*, 22, PA4202, doi:10.1029/2006PA001380, 2007.
- Brovkin, V., Ganopolski, A., Archer, D., and Munhoven, G.: Glacial CO₂ cycle as a succession of key physical and biogeochemical processes, *Clim. Past*, 8, 251–264, doi:10.5194/cp-8-251-2012, 2012.
- Brovkin, V., Brücher, T., Kleinen, T., Zaehle, S., Joos, F., Roth, R., Spahni, R., Schmitt, J., Fischer, H., Leuenberger, M., Stone, E., Ridgwell, A., Chappellaz, J., Khrwald, N., Barbante, C., Blunier, T., and Dahl Jensen, D.: Comparative carbon cycle dynamics of the present and last interglacial, *Quaternary Sci. Rev.*, 137, 15–32, doi:10.1016/j.quascirev.2016.01.028, 2016.
- Buddemeier, R. W. and Smith, S. V.: Coral reef growth in an era of rapidly rising sea level: predictions and suggestions for long-term research, *Coral Reefs*, 7, 51–56, 1988.
- Ciais, P., Sabine, C., Bala, G., Bopp, L., Brovkin, V., Canadell, J., Chhabra, A., DeFries, R., Galloway, J., Heimann, M., Jones, C., Le Quéré, C., Myneni, R. B., Piao, S., and Thornton, P.: Carbon and other biogeochemical cycles, in: *Climate Change 2013: The Physical Science Basis. Contribution of Working Group I to the Fifth Assessment Report of the Intergovernmental Panel on Climate Change*, edited by: Stocker, T. F., Qin, D., Plattner, G.-K., Tignor, M., Allen, S. K., Boschung, J., Nauels, A., Xia, Y., Bex, V., and Midgley, P. M., Cambridge University Press, Cambridge, UK and New York, NY, USA, 465–570, 2013.

- De Kauwe, M. G., Medlyn, B. E., Zaehle, S., Walker, A. P., Dietze, M. C., Wang, Y. P., Luo, Y. Q., Jain, A. K., El-Masri, B., Hickler, T., Warlind, D., Weng, E. S., Parton, W. J., Thornton, P. E., Wang, S. S., Prentice, I. C., Asao, S., Smith, B., McCarthy, H. R., Iversen, C. M., Hanson, P. J., Warren, J. M., Oren, R., and Norby, R. J.: Where does the carbon go? A model-data intercomparison of vegetation carbon allocation and turnover processes at two temperate forest free-air CO₂ enrichment sites, *New Phytol.*, 203, 883–899, 2014.
- Elderfield, H., Ferretti, P., Greaves, M., Crowhurst, S., McCave, I. N., Hodell, D., and Piotrowski, A. M.: Evolution of Ocean Temperature and Ice Volume Through the Mid-Pleistocene Climate Transition, *Science*, 337, 704–709, doi:10.1126/science.1221294, 2012.
- Elsig J., Schmitt J., Leuenberger D., Schneider R., Eyer M., Leuenberger M., Joos F., Fischer H., and Stocker T. F.: Stable isotope constraints on Holocene carbon cycle changes from an Antarctic ice core, *Nature*, 461, 507–510, 2009.
- Frankignoulle, M., Canon, C., and Gattuso, J.-P.: Marine calcification as a source of carbon dioxide: positive feedback of increasing atmospheric CO₂, *Limnol. Oceanogr.*, 39, 458–462, 1994.
- Ganopolski, A. and Calov, R.: The role of orbital forcing, carbon dioxide and regolith in 100kyr glacial cycles, *Clim. Past*, 7, 1415–1425, doi:10.5194/cp-7-1415-2011, 2011.
- Ganopolski, A., Rahmstorf, S., Petoukhov, V., and Claussen, M.: Simulation of modern and glacial climates with a coupled global climate model, *Nature*, 391, 351–356, 1998.
- Ganopolski, A., Petoukhov, V., Rahmstorf, S., Brovkin, V., Claussen, M., Eliseev, A., and Kubatzki, C.: CLIMBER-2: A climate system model of intermediate complexity, Part II: Model sensitivity, *Clim. Dynam.*, 17, 735–751, 2001.
- Gerlach, T.: Volcanic versus anthropogenic carbon dioxide, *Eos Trans. AGU*, 92, 201–202, 2011.
- Gerten D., Schaphoff S., Haberlandt U., Lucht W., and Sitch S.: Terrestrial vegetation and water balance – hydrological evaluation of a dynamic global vegetation model, *J. Hydrol.*, 286, 249–270, 2004.
- Grant, K. M., Rohling, E. J., Bronk Ramsey, C., Cheng, H., Edwards, R. L., Florindo, F., Heslop, D., Marra, F., Roberts, A. P., Tamisiea, M. E., and Williams, F.: Sea-level variability over five glacial cycles, *Nat. Commun.*, 5, 5076, doi:10.1038/ncomms6076, 2014.
- Indermühle, A., Stocker, T. F., Joos, F., Fischer, H., Smith, H. J., Wahlen, M., Deck, B., Mastroianni, D., Tschumi, J., Blunier, T., Meyer, R., and Stauffer, B.: Holocene carbon-cycle dynamics based on CO₂ trapped in ice at Taylor Dome, Antarctica, *Nature*, 398, 121–126, doi:10.1038/18158, 1999.
- Joos, F., Gerber, S., Prentice, I. C., Otto-Bliesner, B. L., and Valdes, P. J.: Transient simulations of Holocene atmospheric carbon dioxide and terrestrial carbon since the Last Glacial Maximum, *Global Biogeochem. Cy.*, 18, GB2002, doi:10.1029/2003GB002156, 2004.
- Kaplan, J. O., Krumhardt, K. M., Ellis, E. C., Ruddiman, W. F., Lemmen, C., and Klein Goldewijk, K.: Holocene carbon emissions as a result of anthropogenic land cover change, *Holocene*, 21, 775–791, doi:10.1177/0959683610386983, 2011.
- Kleinen, T., Brovkin, V., von Bloh, W., Archer, D., and Munhoven, G.: Holocene carbon cycle dynamics, *Geophys. Res. Lett.*, 37, L02705, doi:10.1029/2009GL041391, 2010.
- Kleinen, T., Tarasov, P., Brovkin, V., Andreev, A., and Stebich, M.: Comparison of modeled and reconstructed changes in forest cover through the past 8000 years: Eurasian perspective, *Holocene*, 21, 723–734, doi:10.1177/0959683610386980, 2011.
- Kleinen, T., Brovkin, V., and Schuldt, R. J.: A dynamic model of wetland extent and peat accumulation: results for the Holocene, *Biogeosciences*, 9, 235–248, doi:10.5194/bg-9-235-2012, 2012.
- Kleypas, J. A.: Modeled estimates of global reef habitat and carbonate production since the Last Glacial Maximum, *Paleoceanography*, 12, 533–545, 1997.
- Lourantou, A., Lavrič, J. V., Köhler, P., Barnola, J.-M., Paillard, D., Michel, E., Raynaud, D., and Chappellaz, J.: Constraint of the CO₂ rise by new atmospheric carbon isotopic measurements during the last deglaciation, *Global Biogeochem. Cy.*, 24, GB2015, doi:10.1029/2009GB003545, 2010.
- MacDonald, G. M., Beilman, D. W., Kremenetski, K. V., Sheng, Y., Smith, L. C., and Velichko, A. A.: Rapid Early Development of Circumarctic Peatlands and Atmospheric CH₄ and CO₂ Variations, *Science*, 314, 285–288, doi:10.1126/science.1131722, 2006.
- MacFarling Meure, C., Etheridge, D., Trudinger, C., Steele, P., Langenfelds, R., van Ommen, T., Smith, A., and Elkins, J.: Law Dome CO₂ CH₄ and N₂O ice core records extended to 2000 years BP, *Geophys. Res. Lett.* 33, L14810, doi:10.1029/2006GL026152, 2006.
- Masson-Delmotte, V., Schulz, M., Abe-Ouchi, A., Beer, J., Ganopolski, A., González Rouco, J.F., Jansen, E., Lambeck, K., Luterbacher, J., Naish, T., Osborn, T., Otto-Bliesner, B., Quinn, T., Ramesh, R., Rojas, M., Shao, X., and Timmermann, A.: Information from Paleoclimate Archives, in: *Climate Change 2013: The Physical Science Basis, Contribution of Working Group I to the Fifth Assessment Report of the Intergovernmental Panel on Climate Change*, edited by: Stocker, T. F., Qin, D., Plattner, G.-K., Tignor, M., Allen, S. K., Boschung, J., Nauels, A., Xia, Y., Bex, V., and Midgley, P. M., Cambridge University Press, Cambridge, UK and New York, NY, USA, 383–464, 2013.
- Meinshausen, M., Smith, S. J., Calvin, K. V., Daniel, J. S., Kainuma, M. L. T., Lamarque, J.-F., Matsumoto, K., Montzka, S. A., Raper, S. C. B., Riahi, K., Thomson, A. M., Velders, G. J. M., and van Vuuren, D.: The RCP greenhouse gas concentrations and their extension from 1765 to 2300, *Climatic Change*, 109, 213–241, doi:10.1007/s10584-011-0156-z, 2011.
- Menviel, L. and Joos, F.: Toward explaining the Holocene carbon dioxide and carbon isotope records: results from transient ocean carbon cycle-climate simulations, *Paleoceanography*, 27, PA1207, doi:10.1029/2011PA002224, 2012.
- Milliman, J. D.: Production and accumulation of calcium carbonate in the ocean: Budget of a nonsteady state, *Global Biogeochem. Cy.*, 7, 927–957, 1993.
- Monnin, E., Indermühle, A., Dällenbach, A., Flückiger, J., Stauffer, B., Stocker, T. F., Raynaud, D., and Barnola, J.-M.: Atmospheric CO₂ concentrations over the last glacial termination, *Science*, 291, 112–114, doi:10.1126/science.291.5501.112, 2001.
- Monnin, E., Steig, E.J., Siegenthaler, U., Kawamura, K., Schwander, J., Stauffer, B., Stocker, T. F., Morse, D. L., Barnola, J.-M., Bellier, B., Raynaud, D., and Fischer, H.: Evidence for substantial accumulation rate variability in Antarctica during the Holocene, through synchronization of CO₂ in the Taylor Dome,

- Dome C and DML ice cores, *Earth Planet. Sc. Lett.*, 224, 45–54, doi:10.1016/j.epsl.2004.05.007, 2004.
- Munhoven, G. and François, L. M.: Glacial-interglacial variability of atmospheric CO₂ due to changing continental silicate rock weathering: A model study, *J. Geophys. Res.*, 101, 21423–21437, doi:10.1029/96JD01842, 1996.
- New, M., Hulme, M., and Jones, P.: Representing twentieth-century space-time climate variability, Part II: Development of 1901–96 monthly grids of terrestrial surface climate, *J. Climate*, 13, 2217–2238, 2000.
- Petit, J. R., Jouzel, J., Raynaud, D., Barkov, N. I., Barnola, J.-M., Basile, I., Benders, M., Chappellaz, J., Davis, M., Delayque, G., Delmotte, M., Kotlyakov, V. M., Legrand, M., Lipenkov, V. Y., Lorius, C., Pépin, L., Ritz, C., Saltzman, E., and Stievenard, M.: Climate and atmospheric history of the past 420 000 years from the Vostok ice core, Antarctica, *Nature*, 399, 429–436, 1999.
- Petoukhov, V., A. Ganopolski, V. Brovkin, M. Claussen, A. Eliseev, C. Kubatzki, and Rahmstorf, S.: CLIMBER-2: a climate system model of intermediate complexity, Part I: Model description and performance for present climate, *Clim. Dynam.*, 16, 1–17, 2000.
- Reich, P. B., Hobbie, S. E., and Lee, T. D.: Plant growth enhancement by elevated CO₂ eliminated by joint water and nitrogen limitation, *Nat. Geosci.*, 7, 920–924, 2014.
- Ridgwell, A. J., Watson, A. J., Maslin, M. A., and Kaplan J. O.: Implications of coral reef buildup for the controls on atmospheric CO₂ since the Last Glacial Maximum, *Paleoceanography*, 18, 1083, doi:10.1029/2003PA000893, 2003.
- Rohling, E. J., Braun, K., Grant, K., Kucera, M., Roberts, A. P., Siddall, M., and Trommer, G.: Comparison between Holocene and Marine Isotope Stage-11 sea-level histories, *Earth Planet. Sc. Lett.*, 291, 97–105, doi:10.1016/j.epsl.2009.12.054, 2010.
- Rubino, M., Etheridge, D. M., Trudinger, C. M., Allison, C. E., Battle, M. O., Langenfelds, R. L., Steele, L. P., Curran, M., Bender, M., White, J. W. C., Jenk, T. M., Blunier, T., and Francey, R. J.: A revised 1000 year atmospheric $\delta^{13}\text{C}$ -CO₂ record from Law Dome and South Pole, Antarctica, *J. Geophys. Res.*, 118, 8382–8499, doi:10.1002/jgrd.50668, 2013.
- Ruddiman, W. F.: The anthropogenic greenhouse era began thousands of years ago, *Climatic Change*, 61, 261–293, doi:10.1023/B:CLIM.0000045777.17928.fa, 2003.
- Ruddiman, W. F.: The Anthropocene, *Annu. Rev. Earth Planet. Sci.*, 41, 45–68, doi:10.1146/annurev-earth-050212-123944, 2013.
- Ryan D. A., Opdyke, B. N., and Jell, J. S.: Holocene sediments of Wistari Reef: towards a global quantification of coral reef related neritic sedimentation in the Holocene, *Palaeogeogr. Palaeoclimatol.*, 175, 173–184, 2001.
- Schmitt, J., Schneider, R., Elsig, J., Leuenberger, D., Lourantou, A., Chappellaz, J., Köhler, P., Joos, F., Stocker, T.F., Leuenberger, M., and Fischer, H.: Carbon Isotope Constraints on the Deglacial CO₂ Rise from Ice Cores, *Science*, 336, 711–714, doi:10.1126/science.1217161, 2012.
- Schneider, R., Schmitt, J., Köhler, P., Joos, F., and Fischer, H.: A reconstruction of atmospheric carbon dioxide and its stable carbon isotopic composition from the penultimate glacial maximum to the last glacial inception, *Clim. Past*, 9, 2507–2523, doi:10.5194/cp-9-2507-2013, 2013.
- Schneider von Deimling, T., Meinshausen, M., Levermann, A., Huber, V., Frieler, K., Lawrence, D. M., and Brovkin, V.: Estimating the near-surface permafrost-carbon feedback on global warming, *Biogeosciences*, 9, 649–665, doi:10.5194/bg-9-649-2012, 2012.
- Scholze, M., Kaplan, J. O., Knorr, W., and Heimann, M.: Climate and interannual variability of the atmosphere-biosphere ¹³CO₂ flux, *Geophys. Res. Lett.*, 30, 1097, doi:10.1029/2002GL015631, 2003.
- Schurgers, G., Mikolajewicz, U., Gröger, M., Maier-Reimer, E., Vizcaíno, M., and Winguth, A.: Dynamics of the terrestrial biosphere, climate and atmospheric CO₂ concentration during interglacials: a comparison between Eemian and Holocene, *Clim. Past*, 2, 205–220, doi:10.5194/cp-2-205-2006, 2006.
- Siegenthaler, U., Stocker, T. F., Monnin, E., Lüthi, D., Schwander, J., Stauffer, B., Raynaud, D., Barnola, J.-M., Fischer, H., Masson-Delmotte, V., and Jouzel, J.: Stable carbon cycle-climate relationship during the late pleistocene, *Science*, 310, 1313–1317, 2005.
- Sitch, S., Smith, B., Prentice, I. C., Arneth, A., Bondeau, A., and Cramer, W., Cramer, W., Kaplan, J. O., Levis, S., Lucht, W., Sykes, M. Thonicke, K., and Venevsky, S.: Evaluation of ecosystem dynamics, plant geography and terrestrial carbon cycling in the LPJ dynamic global vegetation model, *Glob. Change Biol.* 9, 161–185, 2003.
- US Department of Commerce: National Oceanic and Atmospheric Administration, National Geophysical Data Center: 2-minute Gridded Global Relief Data (ETOPO2v2), 2006.
- Vecsei, A. and Berger, W. H.: Increase of atmospheric CO₂ during deglaciation: Constraints on the coral reef hypothesis from patterns of deposition, *Global Biogeochem. Cy.*, 18, GB1035, doi:10.1029/2003GB002147, 2004.
- Waelbroeck, C., Labeyrie, L., Michel, E., Duplessy, J. C., McManus, J. F., Lambeck, K., Balbon, E., and Labracherie, M.: Sea-level and deep water temperature changes derived from benthic foraminifera isotopic records, *Quaternary Sci. Rev.*, 21, 295–305, 2002.
- Waite, M. and Sack, L.: Shifts in bryophyte carbon isotope ratio across an elevation × soil age matrix on Mauna Loa, Hawaii: do bryophytes behave like vascular plants?, *Oecologia*, 166, 11–22, doi:10.1007/s00442-010-1903-y, 2011.
- Yu, Z., Loisel, J., Brosseau, D. P., Beilman, D. W., and Hunt, S. J.: Global peatland dynamics since the Last Glacial Maximum, *Geophys. Res. Lett.*, 37, L13402, doi:10.1029/2010GL043584, 2010.